Timing of 29 Pulsars Discovered in the PALFA Survey

A. G. Lyne[1], B. W. Stappers[1], S. Bogdanov[2], R. D. Ferdman[3], P. C. C. Freire[4], V. M. Kaspi[3], B. Knispel[5,6], R. Lynch[3], B. Allen[5,6,7], A. Brazier[8], F. Camilo[9], F. Cardoso[6], S. Chatterjee[8], J. M. Cordes[8], F. Crawford[10], J. S. Deneva[11], J. W. T. Hessels[12,13], F. A. Jenet[14], P. Lazarus[4], J. van Leeuwen[12,13], D. R. Lorimer[15], E. Madsen[3], J. McKee[1], M. A. McLaughlin[15], E. Parent[3], C. Patel[3], S. M. Ransom[16], P. Scholz[3], A. Seymour[4], X. Siemens[6], L. G. Spitler[4], I. H. Stairs[17,3], K. Stovall[18,19], J. Swiggum[6], R. S. Wharton[8], W. W. Zhu[4], C. Aulbert[5,7], O. Bock[5,7], H.-B. Eggenstein[5,7], H. Fehrmann[5,7], B. Machenschalk[5,7]

ABSTRACT

We report on the discovery and timing observations of 29 distant long-period pulsars found in the ongoing Arecibo L-band Feed Array pulsar survey. Following discovery with the Arecibo Telescope, confirmation and timing observations of these pulsars over several years at Jodrell Bank Observatory have yielded high-precision positions and

[1]Jodrell Bank Centre for Astrophys., School of Phys. and Astr., Univ. of Manchester, Manch., M13 9PL, UK

[2]Columbia Astrophysics Laboratory, Columbia Univ., New York, NY 10027, USA

[3]Dept. of Physics and McGill Space Institute, McGill Univ., Montreal, QC H3A 2T8, Canada

[4]Max-Planck-Institut für Radioastronomie, Auf dem Hügel 69, D-53121 Bonn, Germany

[5]Max-Planck-Institut für Gravitationsphysik, D-30167 Hannover, Germany

[6]Physics Dept., Univ. of Wisconsin - Milwaukee, 3135 N. Maryland Ave., Milwaukee, WI 53211, USA

[7]Leibniz Universität Hannover, D-30167 Hannover, Germany

[8]Dept. of Astronomy, Cornell Univ., Ithaca, NY 14853, USA

[9]SKA South Africa, Pinelands, 7405, South Africa

[10]Dept. of Physics and Astronomy, Franklin and Marshall College, Lancaster, PA 17604-3003, USA

[11]National Research Council, resident at the Naval Research Laboratory, Washington, DC 20375, USA

[12]ASTRON, The Netherlands Institute for Radio Astronomy, Postbus 2, 7990 AA, Dwingeloo, The Netherlands

[13]Anton Pannekoek Institute for Astronomy, Univ. of Amsterdam, Science Park 904, 1098 XH Amsterdam, The Netherlands

[14]Center for Gravitational Wave Astronomy, Univ. Texas - Brownsville, TX 78520, USA

[15]Dept. of Physics, West Virginia Univ., Morgantown, WV 26506, USA

[16]NRAO, Charlottesville, VA 22903, USA

[17]Dept. of Physics and Astronomy, Univ. of British Columbia, Vancouver, BC V6T 1Z1, Canada

[18]NRAO, PO Box 0, Socorro, NM 87801, USA

[19]Dept. of Physics and Astronomy, Univ. of New Mexico, NM 87131, USA

measurements of rotation and radiation properties. We have used multi-frequency data to measure the interstellar scattering properties of some of these pulsars. Most of the pulsars have properties that mirror those of the previously known pulsar population, although four show some notable characteristics. PSRs J1907+0631 and J1925+1720 are young and are associated with supernova remnants or plerionic nebulae: J1907+0631 lies close to the center of SNR G40.5−0.5, while J1925+1720 is coincident with a high-energy *Fermi* γ-ray source. One pulsar, J1932+1500, is in a surprisingly eccentric, 199-day binary orbit with a companion having a minimum mass of 0.33 $M_\odot$. Several of the sources exhibit timing noise, and two, PSRs J0611+1436 and J1907+0631, have both suffered large glitches, but with very different post-glitch rotation properties. In particular, the rotational period of PSR J0611+1436 will not recover to its pre-glitch value for about 12 years, a far greater recovery timescale than seen following any other large glitches.

Subject headings: pulsars: general, pulsars: individual: PSR J0611+1436, PSR J1907+0631, PSR J1925+1720, PSR J1932+1500, surveys, ISM: structure; scattering

1. Introduction

The Pulsar Arecibo L-Band Feed Array (PALFA) project is a deep pulsar survey of low Galactic latitudes being conducted at the 305-m William E. Gordon Telescope at the Arecibo Observatory (Cordes et al. 2006; Lazarus et al. 2012; Nice et al. 2013; Lazarus et al. 2015). The survey's relatively high operating frequency of 1420 MHz makes it particularly sensitive to pulsars over a far larger volume of the Galaxy than previous surveys, notably to those pulsars with high dispersion measures (DMs) and short spin periods (Crawford et al. 2012).

The primary aims of the survey include the discovery of binary pulsars which might provide tests of strong-field gravitation theories and the determination of the neutron star equation of state (Stairs 2003; Kramer et al. 2004), the discovery of millisecond pulsars which might be included in pulsar timing arrays in the quest for gravitational waves (Hobbs et al. 2010b), and to better determine the Galactic distribution of the pulsar population (Lorimer et al. 1993; Arzoumanian et al. 2002) and the Galactic interstellar medium (Cordes & Lazio 2002; Han 2004). The properties of PALFA also make it an ideal instrument for discovering young pulsars in the Galactic plane that may have associations with supernova remnants and other high-energy phenomena and are also likely to have notable timing properties for studying neutron star interiors.

In a previous paper, Nice et al. (2013) presented timing measurements of a first tranche of 35 relatively slowly rotating pulsars discovered in the PALFA survey prior to 2008. Here, we describe timing observations of a further 29 such pulsars discovered up to 2013. These observations were made primarily with the Lovell Telescope at Jodrell Bank Observatory, with a few observations using the 100-m Robert C. Byrd Green Bank Telescope. Following a brief description of the survey in Section 2 and presentation of the observations in Section 3, we give the results of timing analyses of the pulsars in Section 4 and provide their flux densities and pulse profiles in Section 5. We also discuss a small number of the pulse profiles which show clear evidence for interstellar multipath scattering. In Sections 6–8, we discuss several notable pulsars: two are young, one is in a binary system, and two display large glitches in their rotation rate. We present our conclusions in Section 9.

2. The PALFA survey

Details of the PALFA survey are described in the following papers: Cordes et al. (2006), van Leeuwen et al. (2006), Lazarus et al. (2012), Nice et al. (2013), Swiggum et al. (2014) and Lazarus et al. (2015). We therefore give only a synopsis here.

The survey includes the regions of the Galactic plane ($|b| < 5°$; $32° \lesssim \ell \lesssim 77°$ and $168° \lesssim \ell \lesssim 214°$) that are accessible with the Arecibo Telescope. Each pointing of the 7-beam ALFA receiver had a dwell time of 268 s and, for observations prior to 2009, a bandwidth of 100 MHz was channelized and digitized using the Wideband Arecibo Pulsar Processor (WAPP) 3-level autocorrelator system (Dowd et al. 2000). The dual polarizations were summed to give 256 total-intensity chan-

nels sampled every 64 μs. Subsequent observations used the wider bandwidth of 322 MHz which was channelized to 960 channels which were sampled every 65.5 μs using the Mock spectrometers (Lazarus et al. 2015). Of the 29 pulsars reported in this paper, 3 were discovered using the WAPP spectrometers and 26 using the Mock spectrometers.

The large volume of data that is acquired has meant that several analysis pipelines were used to process the data and to discover the pulsars by seeking either single or periodic dispersed pulses. Of the pulsars presented in this paper, 13 were discovered using the Einstein@Home pipeline (Allen et al. 2013), which uses spare cycles of a global network of PCs. The other 16 were discovered using either the PRESTO-based pipeline (Ransom 2001; Lazarus et al. 2015), the "Quicklook" pipeline, which runs at the telescope in near-real-time (Cordes et al. 2006), or a pipeline designed to find single dispersed pulses (Deneva et al. 2009).

This paper presents some of the long-period pulsars discovered in the survey to date. However, the survey has already resulted in the discovery of binary and millisecond pulsars (e.g., Lorimer et al. 2006a; Champion et al. 2008; Knispel et al. 2010, 2011, 2015; Crawford et al. 2012; Deneva et al. 2012; Allen et al. 2013; Scholz et al. 2015), as well as the first-known repeating fast radio burst source (Spitler et al. 2014, 2016; Scholz et al. 2016).

3. Confirmation and Timing Observations

The 76-m Lovell Telescope at the Jodrell Bank Observatory, United Kingdom, has been used both to confirm the existence of, and to conduct follow-up timing observations of, more than half of the pulsars detected in the survey, including the 29 pulsars reported here. In addition, one pulsar (J1925+1720) was also observed initially with the Green Bank Telescope. While some of the pulsars we present here were discovered using the single pulse search pipeline, all of the timing solutions presented were derived using the average profiles of each entire observation.

Observations with the Lovell Telescope reported here mostly spanned the period 2011 August and 2015 January (MJD 55800−57050) and made use of a cryogenically cooled dual-polarization receiver working in the frequency range 1350–1700 MHz. The system equivalent flux density on cold sky is 25 Jy. A 512-MHz-wide band was Nyquist sampled at 8-bit resolution and channelized into 0.5-MHz-wide channels using a digital filterbank. To achieve a typical signal-to-noise ratio (S/N) of $\sim 6-10$, observation durations varied from 10 to 40 minutes. For each pulsar the data were folded on to 1024 bins across the pulse period in sub-integrations of 10 s using a polynomial derived from the best ephemeris. The data were "cleaned" of radio-frequency interference by removing sub-integrations or channels that were adversely affected. To form the final average profile, the dispersion delay between the frequency channels was removed using incoherent dedispersion. As the initial period and dispersion measure (DM) values are uncertain, improved pulsar parameters were derived from the confirmation observations by optimising for S/N in the average profile using a range of trial period and DM values. Once these improved parameters were determined, subsequent

analysis used times of arrival (TOAs) with initial phase connection achieved using PSRTIME[1] and final timing solutions were obtained using TEMPO[2]. Each of the sources had an observational cadence of 1–4 weeks depending on telescope availability and typically a single TOA was derived from any given observation.

4. Timing

Timing solutions for each pulsar were found by using TEMPO to fit a standard timing model to the TOAs using a χ^2 minimization technique. To incorporate the TOAs obtained with the Green Bank Telescope for PSR J1925+1720 a time offset was computed between the Jodrell Bank and Green Bank TOAs. Solar system and time transfer made use of the JPL DE405 solar system ephemeris (Standish 1998) and the TT(BIPM) time scale[3] respectively. In all cases the standard model included the rotation period and period derivative, P and $\dot{P}$, the R.A. (J2000) α and Decl. (J2000) δ, and the DM. As discussed below, higher order frequency derivatives, binary parameters and glitch parameters were also needed to adequately model some of the pulsars. The resultant parameters and their associated 95% confidence interval uncertainties are given in Table 1. Although some profiles do show scattering (§5.1), no correction to the DM values for those pulsars has been made.

The timing residuals corresponding to the difference between the measured TOAs and the times of arrival predicted by the timing models are shown in Figures 1 and 2. In the majority of cases the residuals are "white," that is they show no discernible structure. However, in a few cases there is significant timing noise and higher order period derivatives were required to "whiten" the residuals using the method described by Nice et al. (2013). This was necessary in order to measure accurate pulsar parameters. The procedure ensures that the the number of fitted derivatives $n_{\rm fit}$, listed in Table 1, results in groups of timing residuals having no evident correlation.

Several quantities, the spin-down age, $t_{\rm s}$, surface magnetic field strength, B, and spin-down energy loss rates, $\dot{E}$, derived from the timing parameters given in Table 1 are presented in Table 2. The table also contains the Galactic coordinates and the distance derived from the DM and the NE2001 model (Cordes & Lazio 2002) for the distribution of free electrons.

---

[1] `http://www.jb.man.ac.uk/pulsar/observing/progs/psrtime.html`

[2] `http://tempo.sourceforge.net` or `https://github.com/nanograv/tempo`

[3] `ftp://tai.bipm.org/TFG/TT(BIPM)/`

5. Pulse profiles and flux densities

The same Jodrell Bank timing data was used to form a long term average pulse profile and also to determine the mean flux density of all 29 pulsars (Figures 3 and 4). Only observations that resulted in a good TOA were used. The amplitude scale of each pulse profile was adjusted to be in units of the system noise and they were aligned using the "whitened" timing solutions (§4) before being summed.

The system equivalent flux density for each pulsar position was calculated from observations of standard continuum radio sources, adjusted for the local sky brightness temperatures. After appropriate scaling, the time-averaged mean flux density S_{1400} was measured for each profile and is given in Table 1. Luminosity estimates, $L_{1400} = S_{1400}d^2$, are also calculated using the distances derived from DMs using the NE2001 model (Cordes & Lazio 2002) and are given in Table 2.

5.1. Profiles and interstellar scattering

The observed profiles display similar forms to those of the known pulsar population and none exhibits a significant interpulse. The flux density limit for any interpulse emission depends upon the S/N ratio which varies from pulsar to pulsar and can be judged from the profiles presented in Figure 3. This limit is typically 5% of the flux density of the main pulse given in Table 2, assuming that any interpulse has a similar pulse width to that of the main pulse. The widths of the pulse profiles at half the peak height W_{50} in milliseconds are presented in Table 1 and are also typical of the pulsar population.

The relatively high DM values for these pulsars suggests that some of them may show evidence of an asymmetric broadening of the pulse profile with a strong frequency dependence that would be indicative of scattering by the turbulent interstellar medium. As can be seen in Figure 5 this is clearly the case for PSRs J1851+0233, J1859+0603, J1900+0438, and J1901+0459. To quantify the degree of scattering we follow the procedure outlined in Nice et al. (2013), who model the pulse profile as a single Gaussian component convolved with a one-sided exponential that has a e^{-1} broadening time with a frequency dependence given by $\tau_{\rm iss}(f) = \tau_{\rm 1GHz}(f/1\,{\rm GHz})^{-4}$. The amplitude of the Gaussian component is allowed to vary as a function of frequency but the position and width are held fixed. To allow for the fact that the DM used to generate the profiles to be fitted may be biased due to distortions of the pulse shape by the scattering, the model also includes a ΔDM fit parameter to account for this.

This model fitted the observed pulse shapes satisfactorily for all four pulsars. The measured scattering timescales for PSRs J1851+0233, J1859+0603, J1900+0438, and J1901+0459 in the two bands were found to scale with observing frequency approximately as ν^{-4}, confirming the presence of interstellar multipath scattering. The pulse profiles for the four pulsars and their fitted models are shown in Figure 5. The scattering time scales $\tau_{\rm 1GHz}$ were determined with precision of order

ten percent and had values of 0.08(1), 0.09(1), 0.29(3), and 0.12(2) s, respectively. Although this model fits the observed pulse profiles well, we note that it is possible that the intrinsic pulse profiles are more complex than the assumed Gaussian form, and this may have an unrecognized influence on the measured values. In order to provide truer estimates of DM, the values given for the four pulsars in Table 1 include the fitted values of ΔDM.

In addition, PSRs J1857+0300, J1901+0234, and J1903+0654 show some evidence of the expected frequency scaling for scattering, although determination of the amount of scattering was not possible due to the low S/N ratio and/or complex profile morphology. The profiles of the remaining pulsars show no significant scatter broadening.

As noted above, the broadening of the pulse profile can cause the pulses to be delayed by a frequency-dependent amount which results in an overestimate of the DM measured simply by optimising S/N. Such an effect is present even if the pulse-broadening is indiscernible.

6. Young pulsars: PSRs J1907+0631 and J1925+1720

PSRs J1907+0631 and J1925+1720 have the smallest characteristic ages of the 29 pulsars presented, being around 10 kyr and 100 kyr respectively. Further evidence of the youth of PSR J1907+0631 is provided by the fact that it has glitched, as discussed in §8. The ages and locations of the pulsars in the Galactic plane suggest that they might be associated with supernova remnants and/or pulsar wind nebulae. We have therefore studied the regions around each pulsar for such structures.

6.1. PSR J1907+0631

An inspection of Green's catalog (Green 2014) quickly revealed that PSR J1907+0631 is located in SNR G40.5−0.5. In Figure 6 we show a region of the Galactic plane taken from the VLA Galactic Plane Survey (VGPS; Stil et al. (2006)) at 1420 MHz which shows that the pulsar (red cross) is in fact very close to the center (blue cross; R.A. (J2000) = 19:07:08.6, Decl. (J2000) = 06:29:53) of the remnant. We have used the position of the center of the nebula derived by Abdo et al. (2010), which is based on the morphology of the nebula, rather than the previous position obtained by Langston et al. (2000) which was based on single dish radio measurements and which were biased by the bright rim of the asymmetric remnant. It is interesting to note that there appears to be a region of enhanced radio emission at the position of PSR J1907+0631 which might be from a pulsar wind nebula; further multi-wavelength study is required to confirm this.

The age of G40.5–0.5 is often quoted as being 20–40 kyr (Downes et al. 1980) which is broadly consistent with the derived characteristic age of the pulsar. This age is based upon an estimate of the distance to the remnant that ranges between 5.5 and 8 kpc and is derived from various

$\Sigma - D$ relations which relate the diameter of a remnant to its observed radio surface brightness (Clark & Caswell 1976). Yang et al. (2006) study the molecular gas distribution around the remnant and also derive their own $\Sigma - D$ distance of 5.3 kpc. We note that such distances based upon $\Sigma - D$ relationships should be treated with caution (e.g. Green 2015). However, Yang et al. (2006) prefer a distance of 3.4 kpc which they derive from the velocity of a CO feature from shocked gas that they associate with the remnant and the distances from Clemens et al. (1988). This contrasts somewhat with the NE2001-derived distance to the pulsar of 7.9 kpc for the observed DM of 427 pc cm^{-3}. However as can be seen in Figure 6 and discussed in Yang et al. (2006), this is a complex region with many molecular features, while the line of sight to the pulsar and the remnant passes through the nearside of the Sagittarius arm at about 3 kpc and the far side at about 9 kpc.

There has been recent discussion about the possibility that the nearby gamma-ray pulsar J1907+0602 (Abdo et al. 2009) might be associated with G40.5–0.5 because of its association with the nearby TeV source MGRO J1908+06 (Abdo et al. 2007) which extends to include the lower limb of the remnant closest to PSR J1907+0602 (see Figure 1 of Aliu et al. (2014)). Abdo et al. (2010) found that this pulsar (yellow cross in Figure 6) lies in the extended emission seen also with the High Energy Stereoscopic System (HESS; Aharonian et al. 2009) and the Very Energetic Radiation Imaging Telescope Array System (VERITAS; Ward 2008). They noted, however, that the association with G40.5–0.5 seems very unlikely as it would require an extremely high transverse velocity and should have resulted in a bow-shock shaped nebula near the pulsar which was not evident in their *Chandra* X-ray observations. This is consistent with our belief that PSR J1907+0631 is in fact the pulsar that was formed in the G40.5–0.5 supernova event.

The position identified by Abdo et al. (2010) as the center of the remnant seems to be based on the apparently symmetric shape of the nebula. However, they do not quote a position error and the clearly asymmetric intensity distribution of the 1400 MHz radio emission could argue for an offset in the location of the progenitor star from their choice of position. Despite this, we use their position for the purpose of deriving a separation of PSR J1907+0631 from the center of the remnant, which we find to be 1.8 arcminutes. Assuming that the remnant distance is 3.4 kpc and an age for the pulsar of 11 kyr, this separation requires the pulsar to have an unremarkable transverse velocity of 155 km s^{-1}. This would be approximately doubled, and still unremarkable, if the DM-based distance of 7.9 kpc for the pulsar were the true distance. Deeper and higher resolution radio images of the remnant could confirm whether the radio emission close to the pulsar position is indeed a plerion and if it has a bow-shock-like form. The system may then be similar to PSR B1853+01 in W44 (Frail et al. 1996) and we can learn more about the velocity and wind of the pulsar from radio and X-ray (Petre et al. 2002) studies.

PSR J1907+0631 falls within the field of view of an *XMM−Newton* observation which targeted MGRO 1908+06 (ObsID 0553640801). There is no X-ray source detected at the position of the pulsar. Based on the measured DM and DM-derived distance of 7.9 kpc, we estimate the hydrogen column density along the line of sight to PSR J1907+0631 to be $N_{\rm H} \approx 1.3 \times 10^{22}$ cm^{-2} using

the empirical relation from He et al. (2013). Given the non-detection, from the more sensitive EPIC pn data we place a 3σ upper limit on the unabsorbed X-ray luminosity of $L_X \sim 4 \times 10^{32}$ erg s^{-1} in the 0.3–10 keV band. The implied spin-down to X-ray conversion efficiency ($L_X/\dot{E}$) of PSR J1907+0631 is $\lesssim 8 \times 10^{-4}$, which is typical for young pulsars with comparable $\dot{E}$ (see, e.g., Kargaltsev et al. 2012).

6.2. PSR J1925+1720

PSR J1925+1720 is not only youthful but has a sufficiently high $\dot{E}$ that, despite a relatively large NE2001-derived distance of 6.9 kpc, places its $\dot{E}/d^2 = 2.1 \times 10^{34}$ erg kpc^{-2} s^{-1} in the top 10% of all known pulsars. We have therefore sought the presence of any high-energy nebula that might be related to the pulsar.

Inspection of the *Fermi* Large Area Telescope 4-year Point Source Catalog (3FGL; see Acero et al. 2015) reveals that the radio position of PSR J1925+1720 places it 7.4′ from the high-energy γ-ray source 3FGL J1925.4+1727, at R.A. (J2000) = $19^{\rm h}25^{\rm m}29^{\rm s}.6$ Decl. (J2000) = $+17°27'48''$, with a 95% error ellipse of size $6' \times 5.4'$, and position angle $-15.6°$. Although the pulsar falls outside of the error ellipse and the spectrum of 3FGL J1925.4+1727 is not obviously pulsar-like, our investigation indicates that this is caused by the presence of an additional unmodeled source, which appears to be a common occurrence in the Galactic plane (see, e.g., Clark et al. 2015, for the case of PSR J1906+0722).

We note that at X-ray energies, PSR J1925+1720 has been observed with *Swift* XRT for a total effective exposure of 3.4 ks. No sources are apparent in the resulting X-ray image. Taking DM = 223.3 pc cm^{-3} and $d = 6.9$ kpc for the pulsar, we estimate $N_{\rm H} \approx 7 \times 10^{21}$ cm^{-2} as per He et al. (2013). From the available X-ray data, we then obtain a 3σ upper limit of $L_X \sim 2 \times 10^{33}$ erg s^{-1} (0.3–10 keV) on the unabsorbed X-ray luminosity. The implied $L_X/\dot{E} \lesssim 2 \times 10^{-3}$ is consistent with $L_X/\dot{E} = 10^{-4} - 10^{-3}$ observed for analogous energetic pulsars (see Figure 2 in Kargaltsev et al. 2012).

A detailed analysis of the γ-ray emission from PSR J1925+1720 will be presented in a follow-up publication (S. Bogdanov et al. 2016, in preparation).

7. A Long-period pulsar in a 199-day binary orbit: PSR J1932+1500

Shortly after its discovery, timing observations of this 1.86-second pulsar with the Lovell Telescope indicated that the period was changing rapidly, presumably due to the Doppler effect arising from its motion in a binary orbit with a companion star. Subsequent observations confirmed this, and showed it to be in an essentially circular orbit. The parameters resulting from a full fit to the timing data of this pulsar are given in Table 3.

The orbital period, eccentricity and spin characteristics of the PSR J1932+1500 binary system are very similar to those of a previously known pulsar, PSR J1822−0848 (Lorimer et al. 2006b). The spin period and period derivatives of both pulsars indicate that they were only mildly recycled - in the P - $\dot{P}$ diagram they are located in the region where most so-called "normal" pulsars lie. However, as described below they must have experienced some accretion and spin-up.

The orbital eccentricities of these systems (0.0289 and 0.0589 for PSRs J1932+1500 and J1822−0848 respectively) and the estimated companion masses ($\sim 0.30\,M_\odot$ for both systems) provide important clues about their previous evolution. Both eccentricities are much smaller than for truly unrecycled, recently formed pulsars in binary systems, such as PSRs J0045−7319, B1259−63, J1638−4725, J1740−3052, and J2032+4127 (McConnell et al. 1991; Johnston et al. 1992; Lorimer et al. 2006b; Stairs et al. 2001; Lyne et al. 2015), where the pulsars are very young with no signs of significant prior accretion and their massive (from ~ 3 to $\sim 12 M_\odot$) companion stars have not yet entered their giant phases. In these cases, the orbital eccentricities range from 0.6 to 0.96, implying that there has been no time yet for tidal circularization. That will eventually happen when the companion stars evolve into giant stars: their sizes will then be comparable to the minimum orbital separation, and tidal effects will then be very important.

Therefore, it is very likely that the orbits of PSRs J1932+1500 and J1822−0848 have been tidally circularized by their companion in a previous giant stage of their evolution. This was not merely a dynamical interaction – it probably affected the pulsars as well: their P and $\dot{P}$ put them just below the spin period - magnetic field equilibrium line of Pringle & Rees (1972) for accretion at the Eddington rate, i.e. their spin characteristics are consistent with mild accretion by mass transfer from the envelope of the companion. Furthermore, their minimum masses follow the Tauris & Savonije (1999) relation for their orbital periods (see Fig. 4 in that paper).

There are quite a few other moderately recycled pulsars with longer orbital periods that we list in Table 4, the longest being PSR B0820+02 (Manchester et al. 1980), with $P_b = 1232$ days, where the companion is a 0.6-0.7 $M_\odot$ WD (Koester et al. 1992). Many of these binaries (notably PSRs J0214+5222, J2016+1947, J0407+1607, J1711−4322, and J1840−0643) have much shorter spin periods, much smaller B-fields and smaller orbital eccentricities, which places them more in line with the predictions of the convective fluctuation-dissipation theory of Phinney (1992). This is not the case for PSRs J1932+1500 and J1822−0848: although small, their eccentricities are ∼1.5 orders of magnitude larger than the prediction of Phinney (1992), as can be seen in Figure 7.

The reasons for these differences are not clear. Even if PSRs J1932+1500 and J1822−0848 had much stronger B-fields to start with, or perhaps the accretion and related B-field burial was not as efficient, that would not explain why the orbital eccentricities are so much higher than for the other recycled pulsars with wide orbits.

A possible explanation for the characteristics of PSR J1822−0848 was advanced by Tauris et al. (2012). In their scenario, PSR J1822−0848 was initially a non-recycled pulsar in a wide, eccentric orbit. When its companion reached the asymptotic giant branch stage, the system experienced

weak spiral-in (and relatively inefficient orbital circularization) from an almost unbound common envelope. This might explain its spin characteristics (very weak recycling, if at all) and its current orbital period and eccentricity, both of which are much smaller than for the unrecycled pulsar - O-B star systems. This hypothesis would also explain the characteristics of PSR J1932+1500.

The optical characteristics of the companion of PSR J1932+1500 represent an important constraint on the nature and evolution of this system. There is a faint candidate in the SDSS (Alam et al. 2015) at coordinates $\alpha = 19^{\rm h}32^{\rm m}46^{\rm s}.332$, $\delta = +15°00'23''.7$. The angular offset from the pulsar position is $1.3''$; this is significantly larger than the astrometric uncertainties of the catalog (0.15 arcseconds, http://classic.sdss.org/dr7/instruments/technicalPaper/index.html) and more than 3 times the 1-σ positional uncertainty of the pulsar ($0.4''$). This source is not detectable in the 2 micron All-Sky Survey (2MASS, Skrutskie et al. 2006). The significant offset leads us to conclude that the SDSS source is unrelated to the pulsar; its proximity is the result of the large density of stars detected by SDSS in this region of the sky. This non-detection of the companion star suggests that it is a compact object, as predicted by the hypothesis of Tauris et al. (2012).

8. Large glitches in PSRs J0611+1436 and J1907+0631

Timing observations of these two pulsars, with periods of around 0.3 s, showed that they both suffered large glitches in their rotation rates during the timing program, with fractional increases of 5.5×10^{-6} and 2.1×10^{-6}, respectively. However, the evolution of the rotational frequencies and their first derivatives shown in Figure 8, and the relevant parameters summarized in Table 5, reveal that they are very different events.

PSR J1907+0631, with a characteristic age of 11 kyr, is a young Vela-like pulsar, still surrounded by a visible SNR and possibly a plerionic nebula (§6). The observed glitch in this pulsar (Figure 8) is also typical of glitches in the Vela pulsar and similar pulsars such as B1727−33, B1800−21, and B1823−13, having characteristic ages of 10-20 kyr (Lyne et al. 2000; Espinoza et al. 2011). Such glitches are characterized by fractional increases in spin-rate of a few parts per million, followed by a short-term recovery which is completed on a timescale of typically two hundred days, leading into a period of approximately constant $\ddot{\nu}$ until the next glitch occurs. During this last phase, the braking index, $n = \nu\ddot{\nu}/\dot{\nu}^2$, takes a large value of a few 10s, and is about 10 in the case of J1907+0631. This compares with the expected value of $n = 3$ for normal magnetic braking of a rigid neutron star with a constant dipolar magnetic field. Note that the step in rotational frequency at the glitch is seen to be a minor perturbation in the systemic spin-down of the pulsar, and "undoes" only 17 days of spin-down.

On the other hand, it is clear from Figure 8 that PSR J0611+1436, with a characteristic age of 1.1 Myr, shows essentially no short-term transient behavior following the even larger glitch in frequency, and will take ∼12 years to slow down to the pre-glitch rotation rate. This is an extreme recovery time which is not surpassed by glitches in any other normal pulsar, the next largest being

4.9 years in PSR B0355+54 (Lyne 1987) and 4.5 years in B1535−56 (Johnston et al. 1995). Figure 8 also shows that the interglitch rotation rate is dominated by stochastic variations due to timing noise which is prevalent in pulsars of intermediate age (Hobbs et al. 2010a).

The different recovery behavior of glitches between young and intermediate-age pulsars has been pointed out before by Lyne et al. (2000) and studied more recently by Espinoza et al. (2011). It seems that the properties may be related to the decreasing amount of superfluid neutrons as pulsars age. We also note that glitch recoveries in magnetars also show great diversity (Dib & Kaspi 2014) and may also involve changes in the neutron star magnetospheres. In this context, it is notable that PSR J1907+0631 has a large surface magnetic field of just over 10^{13} G, which is greater than that of 98% of the known radio pulsars.

9. Conclusions

The deep search of the Galactic plan undertaken by the PALFA survey has revealed another 29 normal pulsars. The excellent sensitivity of the survey and high frequency resolution of the two data acquisition systems used means that these pulsars have large DMs and are located at a median distance of 7.0 kpc. This value is very similar to the 7.1 kpc of the 35 slow PALFA pulsars presented by Nice et al. (2013), who already noted that this was much larger than the median distance for the known Galactic population of 4.2 kpc (calculated using the ATNF pulsar catalog (Manchester et al. 2005)).

The profiles presented here are indistinct from the normal pulsar population, although a handful do show evidence for scattering and combined with the DM can be added to the PALFA sample to aid in modeling the ionized interstellar medium in the survey region (Nice et al. 2013). This could be enhanced by further observations of this sample at lower frequencies. The combined total of 64 pulsars presented in this paper and in Nice et al. (2013) are just the first of the "normal pulsars" discovered in this survey. The ongoing PALFA survey has to date discovered more than 169 pulsars and, as they probe a unique section of the pulsar population in our Galaxy, they will provide an important statistical sample for modeling the Galactic pulsar population and the distribution of the magneto-ionic medium.

As well as adding to the population as a whole, the sample presented here includes two new young pulsars which both show evidence of interacting with the local medium. PSR J1907+0631 lies close to the center of SNR G40.5–0.5 and thus likely solves the issue of which of the many neutron stars in the area are associated with the remnant. This not only secures another SNR-pulsar association for further detailed study, it clarifies some of the likely properties of pulsars like the gamma-ray source PSR J1907+0602 which had a claim of association. It may also help understand the origin of the TeV emission seen in this region. The youthful and high-$\dot{E}$ pulsar J1925+1720 might be a gamma-ray source or be powering a high-energy nebula. PSR J1907+0631 also exhibited a glitch, as did J0611+1436, and, although they were both large events, they exhibited

very different period and period-derivative evolutions which not only mark them as interesting sources to continue to monitor but also provide important additional data for our understanding of the nature of glitches.

The long period binary pulsar J1932+1500 appears to form a group of two with PSR J1822–0848 that have formed in a system which initially had a wide, eccentric orbit, that underwent only modest spiral in and thus relatively inefficient orbital circularization and likely has a compact companion. This source highlights the wide range of possible outcomes that are possible in the evolution of binary systems which later form at least one neutron star.

The Arecibo Observatory is operated by SRI International under a cooperative agreement with the National Science Foundation (AST-1100968), and in alliance with Ana G. Méndez-Universidad Metropolitana, and the Universities Space Research Association. Pulsar research at Jodrell Bank and access to the Lovell Telescope is supported by a Consolidated Grant from the UK's Science and Technology Facilities Council. This work was supported by the Max Planck Gesellschaft and by NSF grants 1104902, 1105572, and 1148523. P.C.C.F., P.L., and L.G.S. gratefully acknowledge financial support by the European Research Council for the ERC Starting Grant BEACON under contract no. 279702. J.vL. acknowledges funding from the European Research Council under the European Union's Seventh Framework Programme (FP/2007-2013) / ERC Grant Agreement no. 617199. J.S.D. was supported by the NASA Fermi Guest Investigator program and by the Chief of Naval Research. J.W.T.H. acknowledges funding from an NWO Vidi fellowship and from the European Research Council under the European Union's Seventh Framework Programme (FP/2007-2013) / ERC Starting Grant agreement no. 337062 ("DRAGNET"). Pulsar research at UBC is supported by an NSERC Discovery Grant and by the Canadian Institute for Advanced Research. V.M.K. receives support from an NSERC Discovery Grant, an Accelerator Supplement and from the Gerhard Herzberg Award, an R. Howard Webster Foundation Fellowship from the Canadian Institute for Advanced Study, the Canada Research Chairs Program, and the Lorne Trottier Chair in Astrophysics and Cosmology. The National Radio Astronomy Observatory is a facility of the National Science Foundation operated under cooperative agreement by Associated Universities, Inc..

We thank Thomas Tauris for the interesting discussions on the evolution of these pulsars. This research has made use of NASA's Astrophysics Data System Bibliographic Services. We also thank all Einstein@Home volunteers, especially those whose computers found the pulsars with the highest statistical significance. PSR J1855+0306: Jeroen Moetwil, Flagstaff, Arizona, USA and Robert E. Inman Jr., Virginia Beach, Virginia, USA. PSR J1857+0300: "Philemon1752" and "edgen." PSR J1858+0319: Philipp Khlitz, Berlin, Germany and "Termit." PSR J1900+0438: Robert D. Burbeck, Ilkeston, UK and Harald Buchholz, Springfield, Virginia, USA. PSR J1901+0511: John A. Lorimer, Canville, California, USA and Ugur Munir Kir, Istanbul, Turkey. PSR J1903+0654: Paul Frei, Altnau, Switzerland and Jyrki Ojala, Turku, Finland. PSR J1906+0509: Piotr Kamiski, Warsaw (Poland) and "zebo-the-fat." PSR J1907+0859: Naohiro Goto, Ichikawa, Japan and Thomas

Herdtle, St. Paul, Minnesota, USA. PSR J1908+0833: Josef Hahn, Neuss, Germany and Charles Adams, Alamogordo, New Mexico, USA. PSR J1913+1050: Zsolt Szvoboda, Szentendre, Hungary and "Rensk." PSR J1922+1131: Edvin Grabar, Pula, Croatia and Peter van der Spoel, Utrecht, Netherlands. PSR J1954+2407: Andrew Fullford, Dallas, Texas, USA and Pavlo Ovchinnikov, Dnipropetrovsk, Ukraine. PSR J2004+2653: "Cauche Nathanael" and Robert La Plante, Baltimore, Maryland, USA.

REFERENCES

Abdo, A. A., Allen, B., Berley, D., et al. 2007, ApJ, 664, L91

Abdo, A. A., Ackermann, M., Ajello, M., et al. 2009, Science, 325, 840

—. 2010, ApJ, 188, 405

Acero, F., Ackermann, M., Ajello, M., et al. 2015, ApJS, 218, 23

Aharonian, F., Akhperjanian, A. G., Anton, G., et al. 2009, A&A, 499, 723

Alam, S., Albareti, F. D., Allende Prieto, C., et al. 2015, ApJS, 219, 12

Aliu, E., Archambault, S., Aune, T., et al. 2014, ApJ, 787, 166

Allen, B., Knispel, B., Cordes, J. M., et al. 2013, ApJ, 773, 91

Arzoumanian, Z., Chernoff, D. F., & Cordes, J. M. 2002, ApJ, 568, 289

Champion, D., Ransom, S., Lazarus, P., et al. 2008, Science, 320, 1309

Clark, C. J., Pletsch, H. J., Wu, J., et al. 2015, ApJ, 809, L2

Clark, D. H., & Caswell, J. L. 1976, MNRAS, 174, 267

Clemens, D. P., Sanders, D. B., & Scoville, N. Z. 1988, ApJ, 327, 139

Cordes, J. M., & Lazio, T. J. W. 2002, preprint (arXiv:astro-ph/0207156)

Cordes, J. M., Freire, P. C. C., Lorimer, D. R., et al. 2006, ApJ, 637, 446

Crawford, F., Stovall, K., Lyne, A. G., et al. 2012, ApJ, 757, 90

Deneva, J. S., Cordes, J. M., McLaughlin, M. A., et al. 2009, ApJ, 703, 2259

Deneva, J. S., Freire, P. C. C., Cordes, J. M., et al. 2012, ApJ, 757, 89

Dib, R., & Kaspi, V. M. 2014, ApJ, 784, 37

Dowd, A., Sisk, W., & Hagen, J. 2000, in Pulsar Astronomy - 2000 and Beyond, IAU Colloquium 177, ed. M. Kramer, N. Wex, & R. Wielebinski (San Francisco: Astronomical Society of the Pacific), 275–276

Downes, A. J. B., Salter, C. J., & Pauls, T. 1980, A&A, 92, 47

Espinoza, C. M., Lyne, A. G., Stappers, B. W., & Kramer, M. 2011, MNRAS, 414, 1679

Frail, D. A., Giacani, E. B., Goss, W. M., & Dubner, G. 1996, ApJ, 464, L165

Green, D. A. 2014, Bulletin of the Astronomical Society of India, 42, 47

—. 2015, MNRAS, 454, 1517

Han, J. L. 2004, in The Magnetized Interstellar Medium, ed. B. Uyaniker, W. Reich, & R. Wielebinski, 3–12

He, C., Ng, C.-Y., & Kaspi, V. M. 2013, ApJ, 768, 64

Hobbs, G., Lyne, A. G., & Kramer, M. 2010a, MNRAS, 402, 1027

Hobbs, G., Archibald, A., Arzoumanian, Z., et al. 2010b, Classical and Quantum Gravity, 27, 084013

Johnston, S., Lyne, A. G., Manchester, R. N., et al. 1992, MNRAS, 255, 401

Johnston, S., Manchester, R. N., Lyne, A. G., Kaspi, V. M., & D'Amico, N. 1995, A&A, 293, 795

Kargaltsev, O., Durant, M., Pavlov, G. G., & Garmire, G. 2012, ApJS, 201, 37

Knispel, B., Allen, B., Cordes, J. M., et al. 2010, Science, 329, 1305

Knispel, B., Lazarus, P., Allen, B., et al. 2011, ApJ, 732, L1

Knispel, B., Lyne, A. G., Stappers, B. W., et al. 2015, ApJ, 806, 140

Koester, D., Chanmugam, G., & Reimers, D. 1992, ApJ, 395, L107

Kramer, M., Backer, D. C., Cordes, J. M., et al. 2004, New Astronomy Reviews, 48, 993

Langston, G., Minter, A., D'Addario, L., et al. 2000, AJ, 119, 2801

Lazarus, P., Allen, B., Bhat, N. D. R., et al. 2012, in IAU Symposium 291: Neutron Stars and Pulsars: Challenges and Opportunities after 80 years, ed. J. van Leeuwen

Lazarus, P., Brazier, A., Hessels, J. W. T., et al. 2015, ApJ, 812, 81

Lorimer, D. R., Bailes, M., Dewey, R. J., & Harrison, P. A. 1993, MNRAS, 263, 403

Lorimer, D. R., Stairs, I. H., Freire, P. C., et al. 2006a, ApJ, 640, 428

Lorimer, D. R., Faulkner, A. J., Lyne, A. G., et al. 2006b, MNRAS, 372, 777

Lyne, A. G. 1987, Nature, 326, 569

Lyne, A. G., Shemar, S. L., & Graham-Smith, F. 2000, MNRAS, 315, 534

Lyne, A. G., Stappers, B. W., Keith, M. J., et al. 2015, MNRAS, 451, 581

Manchester, R. N., Hobbs, G. B., Teoh, A., & Hobbs, M. 2005, AJ, 129, 1993

Manchester, R. N., Newton, L. M., Cooke, D. J., & Lyne, A. G. 1980, ApJ, 236, L25

McConnell, D., McCulloch, P. M., Hamilton, P. A., et al. 1991, MNRAS, 249, 654

Nice, D. J., Altiere, E., Bogdanov, S., et al. 2013, ApJ, 772, 50

Petre, R., Kuntz, K. D., & Shelton, R. L. 2002, ApJ, 579, 404

Phinney, E. S. 1992, Phil. Trans. Roy. Soc. A, 341, 39

Pringle, J. E., & Rees, M. J. 1972, A&A, 21, 1

Ransom, S. M. 2001, PhD thesis, Harvard University

Scholz, P., Kaspi, V. M., Lyne, A. G., et al. 2015, ApJ, 800, 123

Scholz, P., Spitler, L. G., Hessels, J. W. T., et al. 2016, ArXiv e-prints, arXiv:1603.08880

Skrutskie, M. F., Cutri, R. M., Stiening, R., et al. 2006, AJ, 131, 1163

Spitler, L. G., Cordes, J. M., Hessels, J. W. T., et al. 2014, ApJ, 790, 101

Spitler, L. G., Scholz, P., Hessels, J. W. T., et al. 2016, Nature, 531, 202

Stairs, I. H. 2003, Living Reviews in Relativity, 5, URL (Cited on 2008/02/16): http://relativity.livingreviews.org/Articles/lrr-2003-5

Stairs, I. H., Manchester, R. N., Lyne, A. G., et al. 2001, MNRAS, 325, 979

Standish, E. M. 1998, JPL Planetary and Lunar Ephemerides, DE405/LE405, Memo IOM 312.F-98-048 (Pasadena: JPL), http://ssd.jpl.nasa.gov/iau-comm4/de405iom/de405iom.pdf

Stil, J. M., Taylor, A. R., Dickey, J. M., et al. 2006, AJ, 132, 1158

Swiggum, J. K., Lorimer, D. R., McLaughlin, M. A., et al. 2014, ApJ, 787, 137

Tauris, T. M., Langer, N., & Kramer, M. 2012, MNRAS, 425, 1601

Tauris, T. M., & Savonije, G. J. 1999, A&A, 350, 928

van Leeuwen, J., Cordes, J. M., Lorimer, D. R., et al. 2006, Chinese Journal of Astronomy and Astrophysics, 6, 311

Ward, J. E. 2008, in AIP Conference Series, Vol. 1085, ed. F. A. Aharonian, W. Hofmann, & F. Rieger, 301–303

Yang, J., Zhang, J.-L., Cai, Z.-Y., Lu, D.-R., & Tan, Y.-H. 2006, Chinese Journal of Astronomy and Astrophysics, 6, 210

Table 1. Measured Parameters of 29 Pulsars[a]

PSR	α (J2000)	δ (J2000)	Epoch (MJD)	P (s)	$\dot{P}$ (10^{-15})	DM ($\mathrm{pc\,cm^{-3}}$)	n_{fit}	σ_{res} (ms)	S_{1400} (mJy)	W_{50} (ms)
J0611+1436	06:11:18.649(13)	+14:36:52(4)	55818	0.27032946262(3)	3.997(3)	45.7(7)	9	1.2	1.10	11.6
J1851+0233	18:51:09.130(19)	+02:33:46.4(9)	56700	0.344018308374(12)	2.1844(13)	606(4)[b]	1	1.8	0.08	13.5
J1854+0319	18:54:00.110(12)	+03:19:12.8(5)	56700	0.628540823296(15)	0.0551(6)	480.2(13)	1	1.0	0.17	10.4
J1855+0306	18:55:38.24(7)	+03:06:22(3)	56700	1.63356517930(18)	6.971(8)	634(6)	2	5.0	0.06	35.9
J1857+0300	18:57:16.91(3)	+03:00:26.0(13)	56700	0.77267804332(4)	2.6489(16)	691(4)	1	2.8	0.05	14.0
J1858+0319	18:58:40.88(3)	+03:19:21.5(10)	56700	0.86744387855(4)	0.1025(15)	284(3)	1	2.7	0.06	10.6
J1859+0603	18:59:42.131(16)	+06:03:54.5(5)	56700	0.508561079708(17)	1.5895(10)	378.6(20)[b]	1	1.1	0.16	13.8
J1900+0438	19:00:13.35(3)	+04:38:46.8(11)	56700	0.312314406456(18)	3.2304(8)	627(6)[b]	1	3.0	0.12	26.0
J1901+0234	19:01:26.93(3)	+02:34:51.4(10)	56700	0.88524028123(4)	23.034(4)	404(3)	1	2.9	0.14	20.4
J1901+0459	19:01:17.47(4)	+04:59:06.8(12)	56700	0.87704381015(6)	15.6817(20)	1108(4)[b]	1	2.9	0.12	28.0
J1901+0511	19:01:42.91(5)	+05:11:00.2(15)	56700	4.6003689902(4)	25.338(15)	410(7)	1	2.0	0.05	23.5
J1903+0654	19:03:55.28(5)	+06:54:39.4(16)	56700	0.79123225301(7)	10.595(4)	329(7)	1	3.3	0.11	56.2
J1906+0509	19:06:56.497(16)	+05:09:35.6(6)	56406	0.397589683040(5)	5.2152(4)	99.5(19)	1	1.3	0.07	21.2
J1907+0255	19:07:17.90(4)	+02:55:02.7(10)	56700	0.61876063644(3)	0.2230(9)	257(4)	1	3.3	0.14	30.8
J1907+0631	19:07:03.816(17)	+06:31:18.9(6)	56985	0.323648024490(19)	452.1551(12)	428.6(18)	4	2.0	0.25	14.8
J1907+0859	19:07:01.913(10)	+08:59:43.8(4)	56700	1.52704227084(3)	5.5446(12)	190(3)	1	0.9	0.07	35.6
J1908+0833	19:08:20.960(16)	+08:33:31.5(5)	56700	0.512110722994(12)	1.9872(7)	700.1(20)	1	1.4	0.20	14.6
J1909+1148	19:09:31.379(3)	+11:48:59.86(8)	56700	0.448945466859(3)	0.07250(8)	199.8(5)	1	0.3	0.09	4.6
J1913+0657	19:13:32.92(4)	+06:57:24.3(10)	56700	1.25718110369(7)	2.829(7)	142(3)	1	1.3	0.05	19.4
J1913+1050	19:13:35.364(9)	+10:50:26.6(3)	56700	0.190067107649(3)	0.19546(12)	231.1(9)	1	0.7	0.06	4.5
J1922+1131	19:22:50.27(3)	+11:31:58.5(6)	56700	0.56207429041(3)	0.0257(10)	335(3)	1	2.4	0.13	23.0
J1925+1720	19:25:27.031(4)	+17:20:27.31(8)	56700	0.0756589884532(11)	10.46782(11)	223.3(15)	4	0.3	0.07	2.2
J1928+1443	19:28:06.79(5)	+14:43:11.3(12)	56700	1.01073895346(7)	0.210(8)	101(5)	1	3.4	0.17	41.6
J1931+1439	19:31:40.433(18)	+14:39:38.7(4)	56700	1.77922557495(7)	6.328(2)	243(16)	1	1.1	0.08	64.2
J1932+1500	19:32:46.307(15)	+15:00:22.2(4)	56700	1.86433186749(10)	0.459(6)	90.5(18)	1	1.0	0.19	50.7
J1940+2245	19:40:27.644(10)	+22:45:46.62(20)	56700	0.258911996567(5)	12.71254(19)	222.4(13)	1	1.3	0.15	13.0
J1948+2333	19:48:19.317(3)	+23:33:03.23(5)	56050	0.5283521633015(16)	13.57843(4)	198.2(8)	2	1.9	0.28	5.2
J1954+2407	19:54:00.374(3)	+24:07:14.00(4)	56700	0.1934045707829(15)	1.05616(7)	80.5(4)	3	0.4	0.10	1.9
J2004+2653	20:04:59.02(4)	+26:53:40.4(6)	56700	0.66587861963(4)	0.0567(12)	160(4)	2	2.4	0.06	14.8

[a]Figures in parentheses are uncertainties in the last digit quoted.

[b]The value of DM has been adjusted for the effects of interstellar scatter broadening (Section 5.1).

Table 2. Derived Parameters of 29 Pulsars

PSR	l (°)	b (°)	DM (pc cm^{-3})	d^{a} (kpc)	L_{1400} (mJy kpc^2)	log t_c (log yr)	log B (log G)	log $\dot{E}$ (log erg/s)
J0611+1436	195.38	−2.00	45.7	1.5	2.4	6.03	12.0	33.9
J1851+0233	35.18	1.23	608.2	11.0	9.6	6.40	11.9	33.3
J1854+0319	36.18	0.94	480.2	8.5	12.3	8.26	11.3	30.9
J1855+0306	36.17	0.48	634.3	9.4	5.4	6.57	12.5	31.8
J1857+0300	36.27	0.07	691.0	9.8	4.7	6.66	12.2	32.4
J1858+0319	36.71	−0.09	283.7	6.1	2.2	8.13	11.5	30.8
J1859+0603	39.27	0.93	382.1	7.4	8.7	6.70	12.0	32.7
J1900+0438	38.07	0.17	630.5	9.5	10.3	6.19	12.0	33.6
J1901+0234	36.37	−1.05	404.3	7.4	7.3	5.78	12.7	33.1
J1901+0459	38.49	0.09	1112.3	≥20.0	≥45.2	5.95	12.6	33.0
J1901+0511	38.71	0.08	410.1	7.1	2.3	6.46	13.0	31.0
J1903+0654	40.50	0.39	328.8	6.8	4.9	6.07	12.5	32.9
J1906+0509	39.29	−1.08	99.5	3.5	0.8	6.08	12.2	33.5
J1907+0255	37.34	−2.19	256.9	6.1	5.4	7.64	11.6	31.6
J1907+0631	40.51	−0.48	428.6	7.9	15.5	4.05	13.1	35.7
J1907+0859	42.71	0.66	190.0	5.2	1.8	6.64	12.5	31.8
J1908+0833	42.47	0.17	700.1	12.8	15.8	6.61	12.0	32.8
J1909+1148	45.49	1.42	199.8	5.7	2.8	7.99	11.3	31.5
J1913+0657	41.64	−1.71	142.2	4.6	1.1	6.85	12.3	31.8
J1913+1050	45.09	0.08	231.1	6.0	2.2	7.19	11.3	33.1
J1922+1131	46.76	−1.60	335.1	9.1	10.5	8.54	11.1	30.8
J1925+1720	52.18	0.59	223.3	6.9	3.4	5.06	12.0	36.0
J1928+1443	50.18	−1.22	100.9	4.3	3.1	7.88	11.7	30.9
J1931+1439	50.54	−2.00	242.9	7.7	4.7	6.65	12.5	31.6
J1932+1500	50.97	−2.07	90.5	3.7	2.5	7.81	12.0	30.4
J1940+2245	58.63	0.13	222.4	7.4	8.3	5.51	12.3	34.5
J1948+2333	60.21	−1.04	198.2	7.1	13.7	5.79	12.4	33.6
J1954+2407	61.37	−1.87	80.5	3.9	1.5	6.46	11.7	33.8
J2004+2653	65.03	−2.53	159.7	6.3	2.3	8.27	11.3	30.9

[a]Values predicted based on l, b, and DM, using the NE2001 electron density model of Cordes & Lazio (2002).

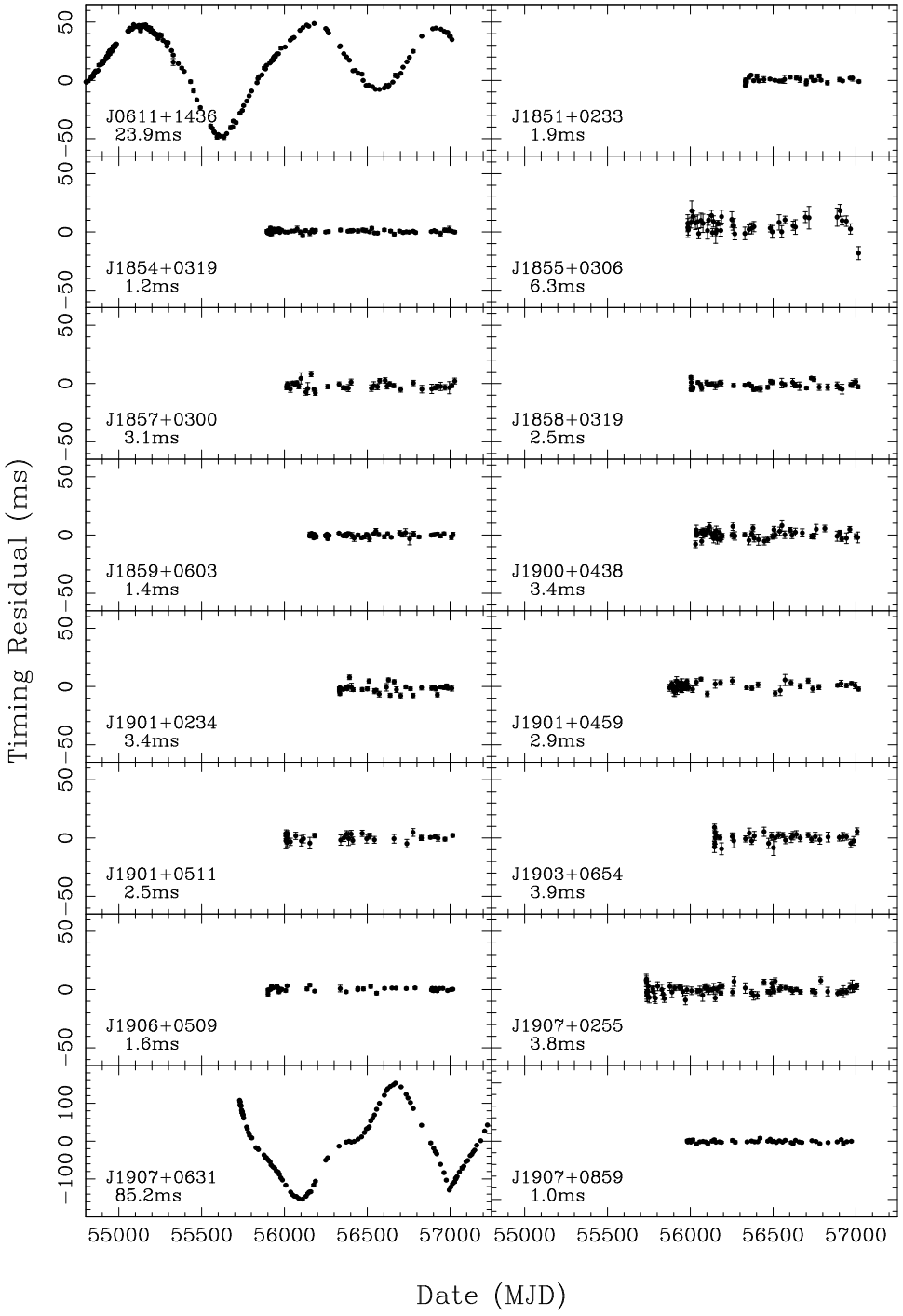

Fig. 1.— Residual pulse arrival times of all pulsars in this paper are given in Figures 1 and 2 to indicate the levels of timing noise. For each pulsar, the residual plot was made by performing a timing fit for just spin-period and spin-down rate, with the best-fit positions given in Table 1 and any binary or glitch parameters given in Tables 3 or 5 held fixed. The root-mean-square of the residuals is given beneath each pulsar name.

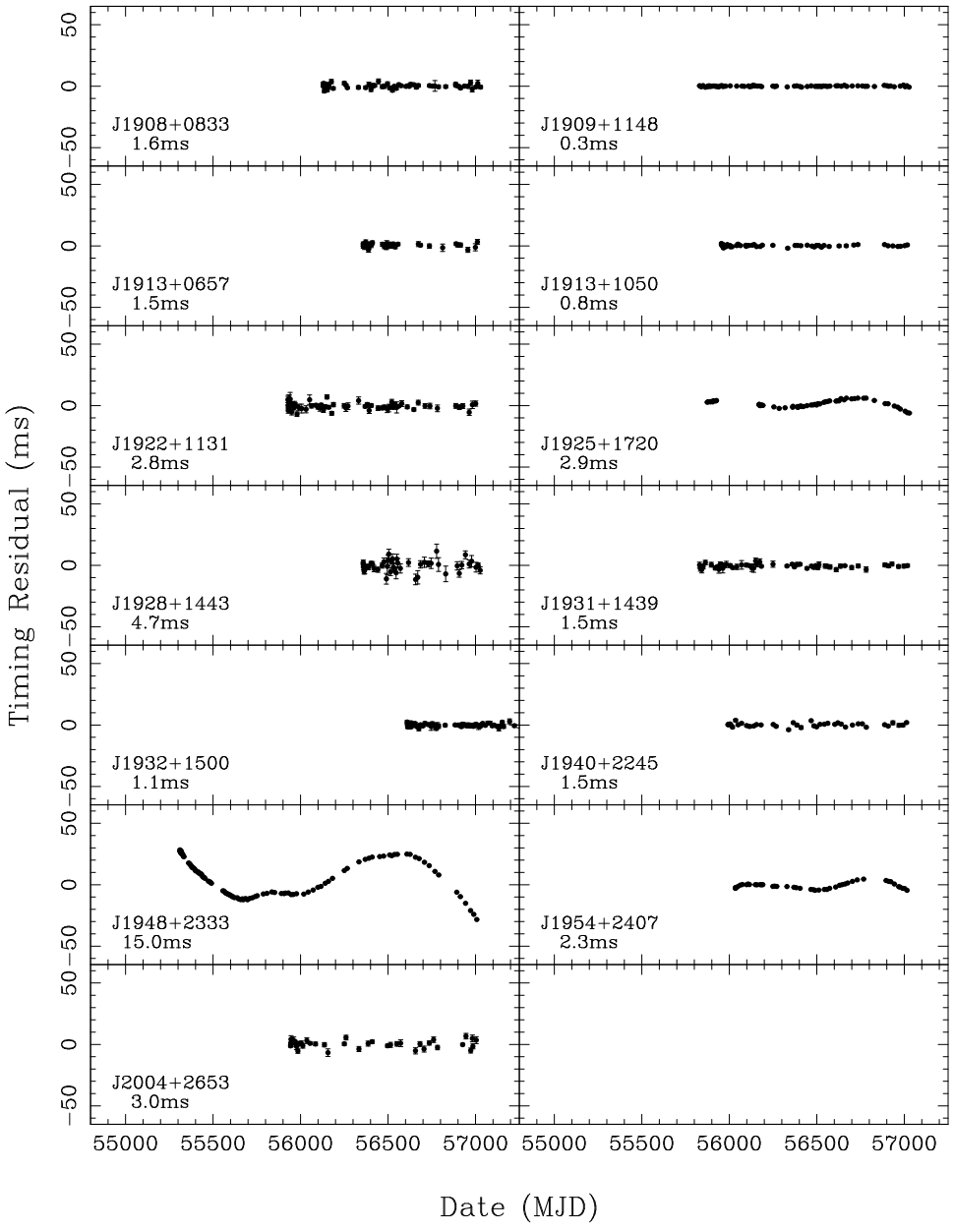

Fig. 2.— See the caption for Figure 1.

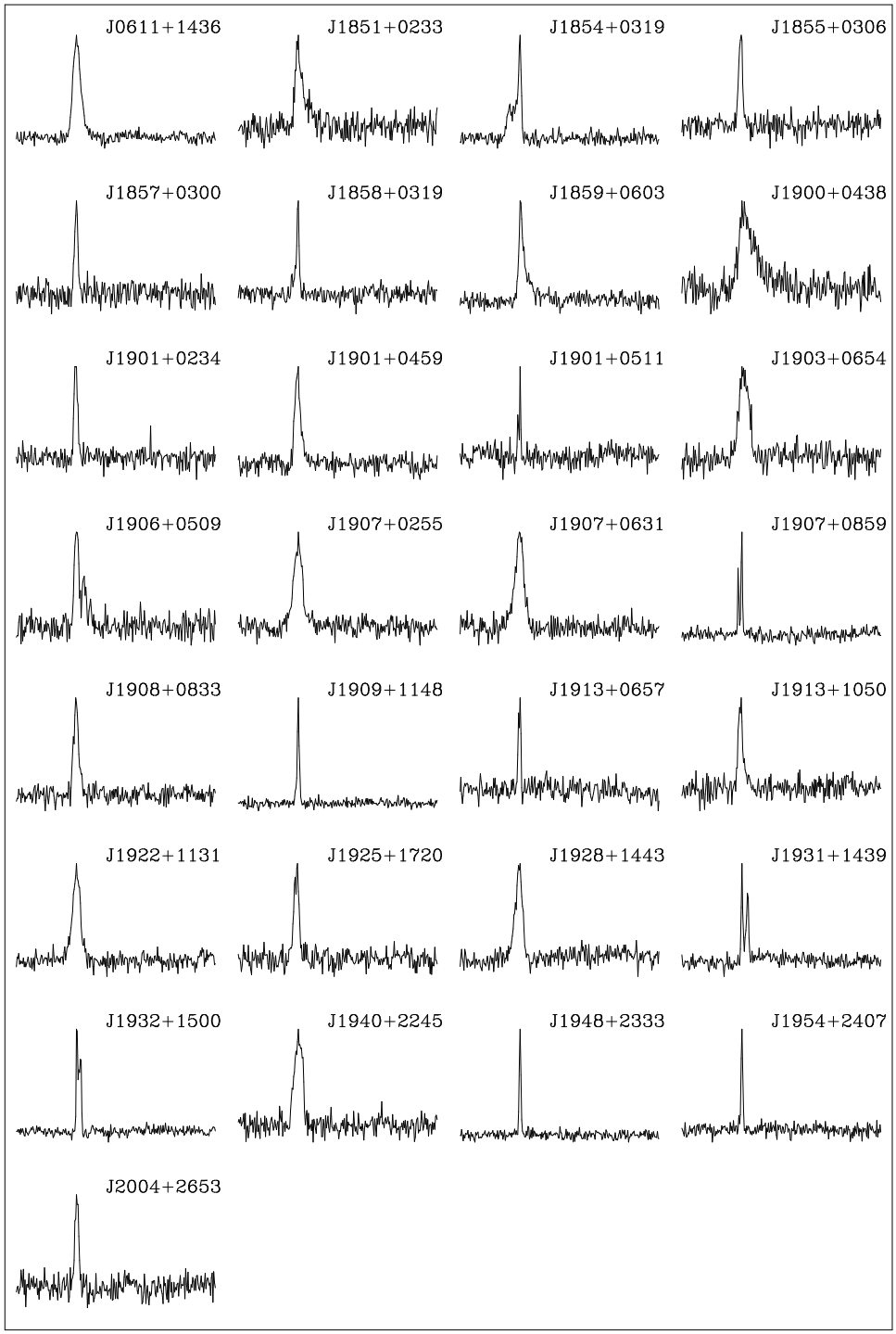

Fig. 3.— Total-intensity profiles for each of the 29 pulsars. The full pulse period is shown and all the profiles have been averaged to 256 bins. All observations that contributed to the average profile used the whitened timing solution for alignment prior to summation. In all cases there is no significant broadening due to the instrument or dispersion smearing. The region around the pulse peaks is shown in more detail in Figure 4. The profiles of the 29 pulsars presented in this paper and those from Nice et al. (2013) are available from the EPN database (http://www.epta.eu.org/epndb/)

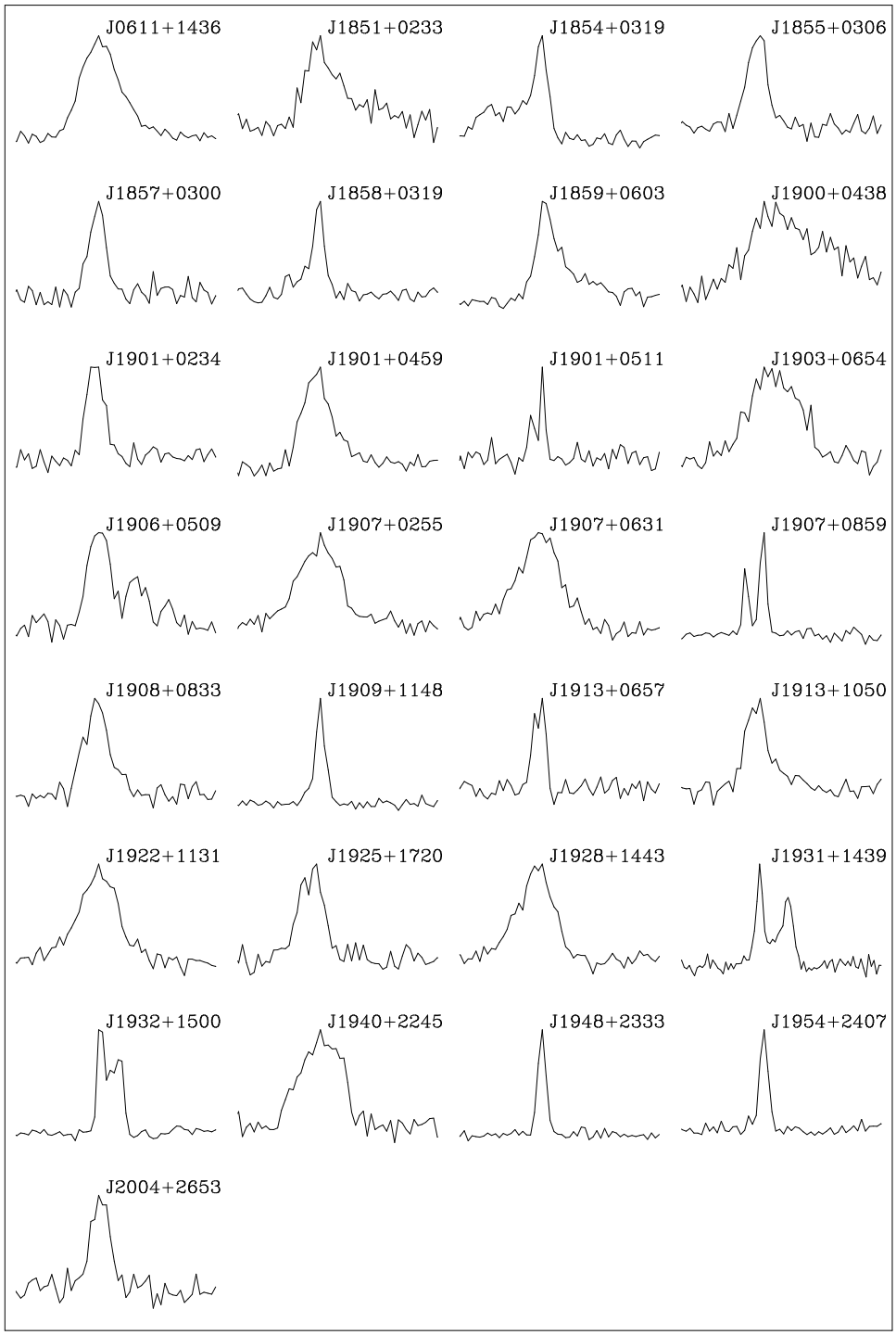

Fig. 4.— The same pulse profiles as presented in Figure 3 but now expanded to show the 20% of the profile around the main peak.

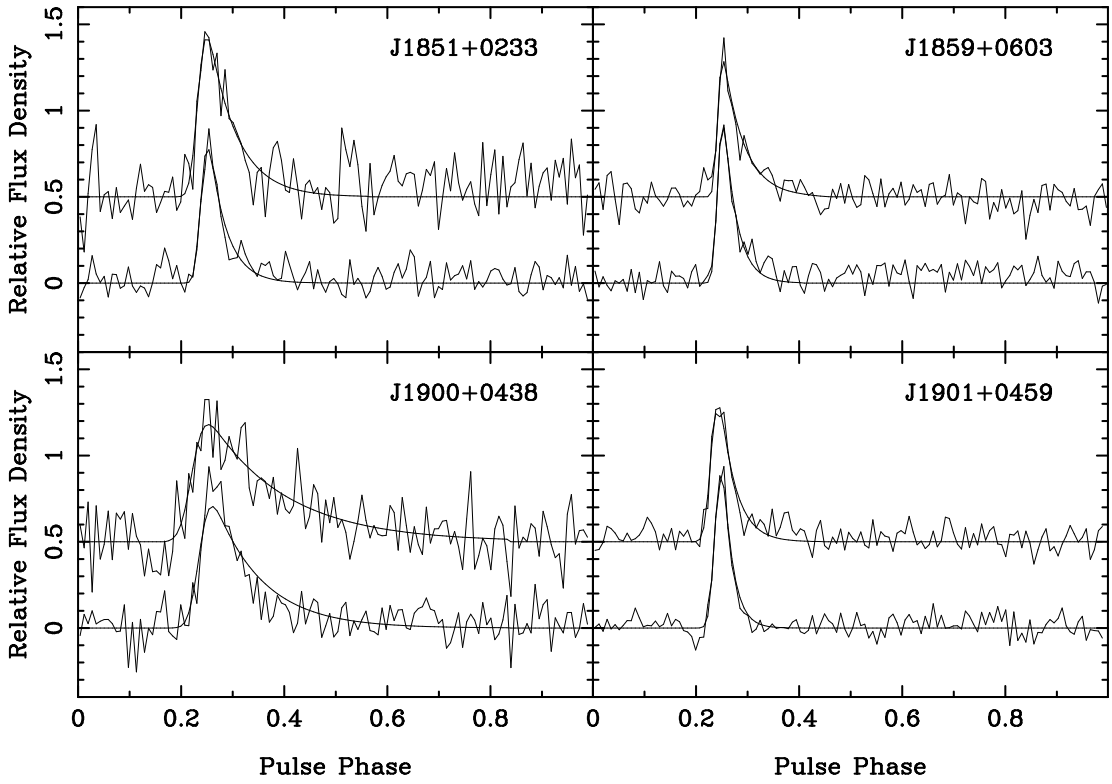

Fig. 5.— Pulse profiles from PSRs J1851+0233, J1859+0603, J1900+0438 and J1901+0459 exhibiting broadening due to scattering in the interstellar medium. In each frame, the upper and lower profiles are centered on 1450 MHz and 1650 MHz, respectively. The smooth curves are the best-fit model, see the text for details, to the displayed profiles.

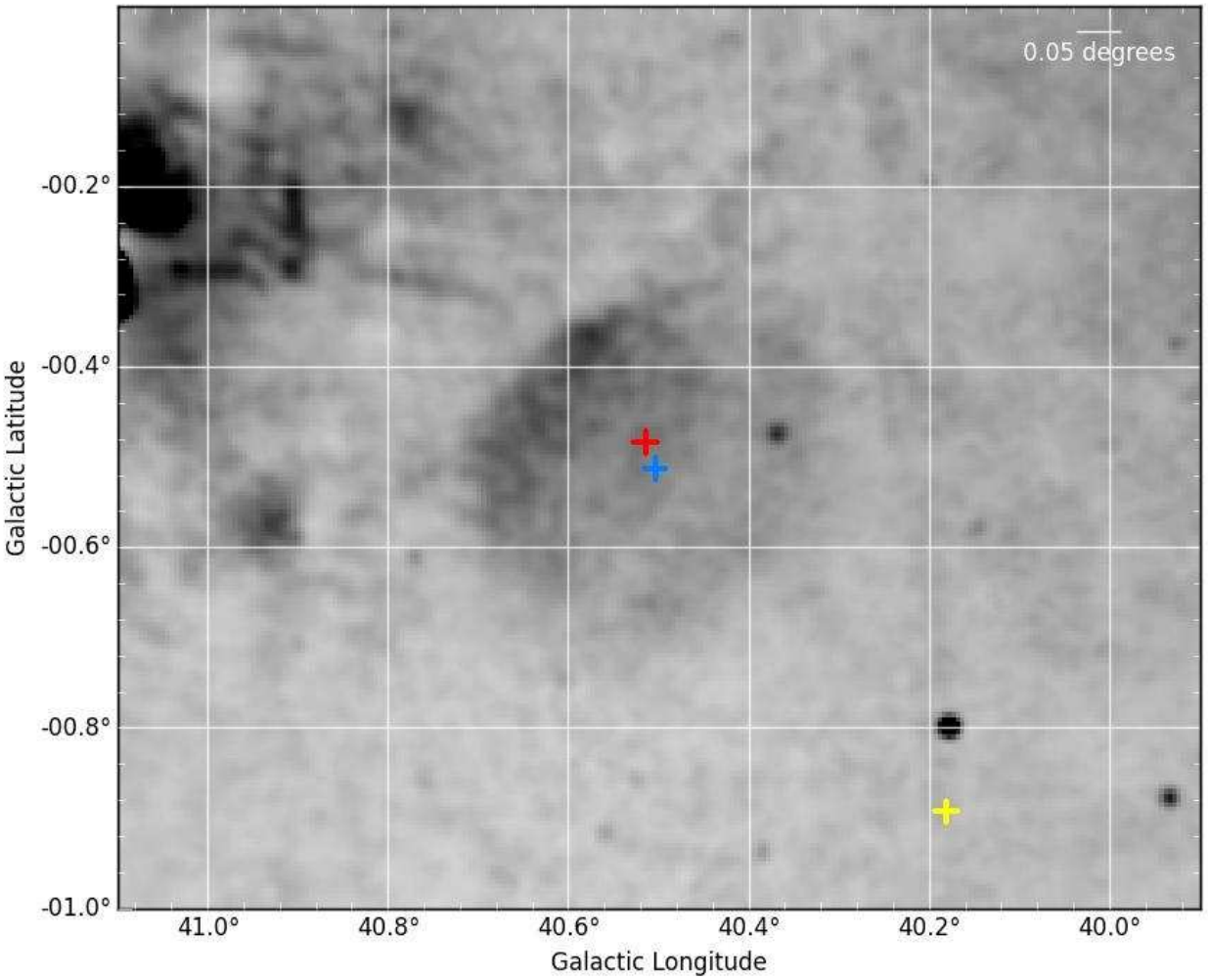

Fig. 6.— A radio image of the region around PSR J1907+0631 in galactic coordinates, taken from the VGPS at 1420 MHz (Stil et al. 2006). The red cross is the position of the pulsar, the blue cross is the center of the supernova remnant G40.5−0.5 given by Abdo et al. (2010) and the yellow cross is the position of the gamma-ray pulsar, PSR J1907+0602.

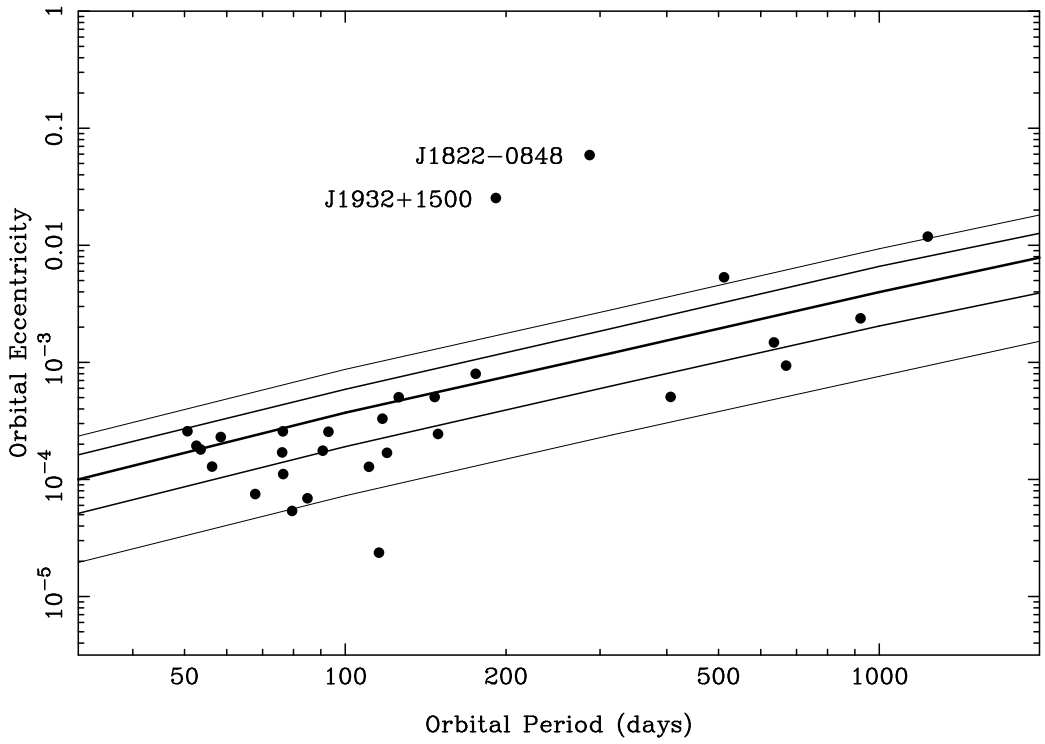

Fig. 7.— The anomalous eccentricities of PSRs J1932+1500 and PSR 1822−0848, compared with those of other long-period, mildly recycled pulsars and the predictions of Phinney (1992). This diagram includes all known Galactic binary pulsars with orbital period greater than 50 days and minimum companion mass less than 0.5 $M_\odot$ (Table 4). The central curve represents the median eccentricity predicted by the convective fluctuation-dissipation theory of Phinney (1992). The adjacent pairs of lines are predicted to contain 68% and 95% of the resultant eccentricities. Excluding PSRs J1932+1500 and PSR 1822−0848, the observed occupancies of the two ranges are 56% and 85% respectively and are reasonably consistent with the theory.

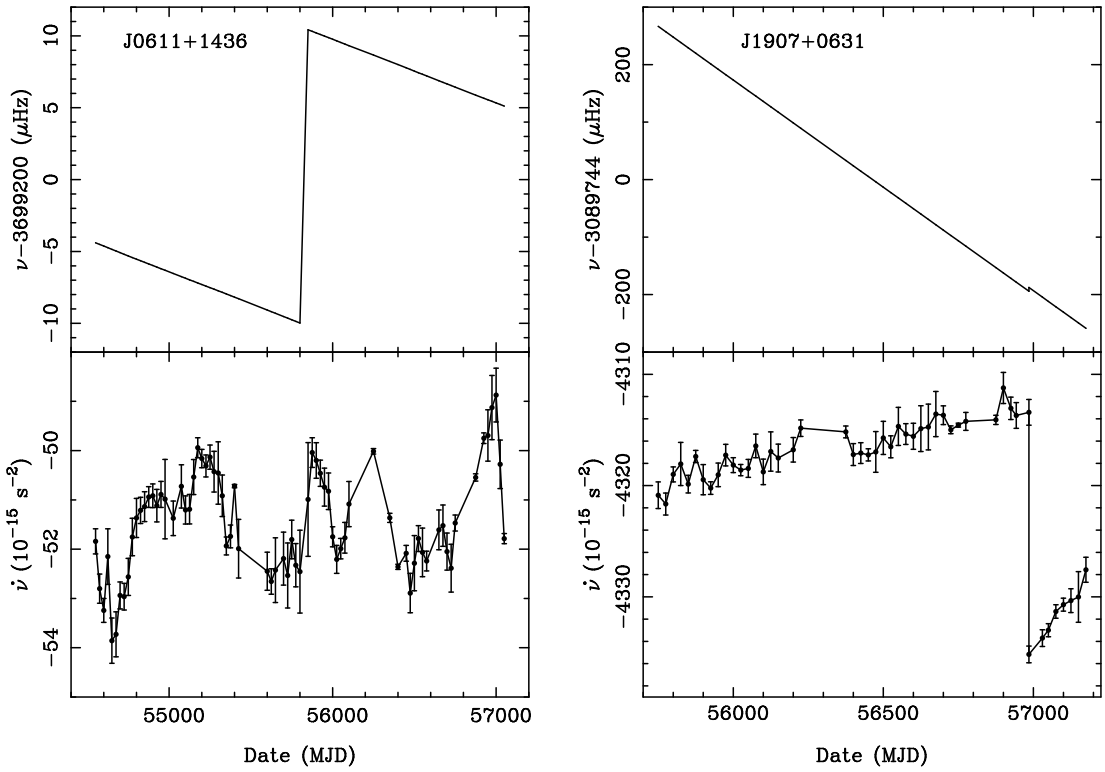

Fig. 8.— The large glitches in PSR J0611+1436 and PSR 1907+0631. Top: the evolution of the rotation frequency ν. Bottom: the evolution of the frequency derivative $\dot{\nu}$. Note that in PSR J0611+1436, the glitch reverses approximately 12 years of normal spin down, compared with 17 days in PSR 1907+0631.

Table 3. Observed and derived parameters of the binary pulsar PSR J1932+1500[a]

	PSR J1932+1500
Right Ascension (J2000)	19:32:46.307(16)
Declination (J2000)	+15:00:22.2(4)
Epoch of pulsar period (MJD)	56700
Pulsar rotation period (s)	1.8643318675(2)
Pulsar rotation frequency (s^{-1})	0.53638518841(3)
First derivative of pulsar frequency (s^{-2})	$-0.132(2) \times 10^{-15}$
Binary Period (d)	198.9251(2)
Epoch of Periastron (MJD)	56634.898(14)
Orbital semi-major axis (s)	76.9255(6)
Eccentricity	0.028928(14)
Longitude of periastron (°)	292.13(2)
Binary mass function	0.0123 $M_\odot$
Spin-down age (Myr)	64.4
Spin-down energy (erg/s)	2.5×10^{30}
Inferred Magnetic Field (G)	1×10^{12}
Distance (kpc)[b]	3.7

[a]Figures in parentheses are uncertainties in the last digit quoted.

[b]Value predicted based on l, b, and DM, using the NE2001 electron density model of Cordes & Lazio (2002).

Table 4. Wide-orbit binary pulsars. Together with PSR J1932+1500 reported here, these are all known Galactic binary pulsars taken from the ATNF Pulsar Catalogue (Manchester et al. 2005) which have orbital period greater than 50 d and minimum companion mass less than 0.5 $M_\odot$. The two pulsars with anomalously high values of eccentricity and which are discussed in the text are highlighted in bold font.

PSR	P(s)	P_b(days)	Ecc	$M_c(M_\odot)$	B(TG)
B0820+02	0.864873	1232.404	0.01187	0.19	0.304
J1711−4322	0.102618	922.471	0.002376	0.20	0.0529
J0407+1607	0.025702	669.070	0.000936	0.19	0.00144
J2016+1948	0.064940	635.024	0.001480	0.29	0.00516
J0214+5222	0.024575	512.040	0.005328	0.41	0.00274
B1800−27	0.334415	406.781	0.000507	0.14	0.0766
J1822−0848	**2.504518**	**286.830**	**0.05896**	**0.32**	**1.02**
J1932+1500	**1.864332**	**198.925**	**0.028924**	**0.32**	**0.0529**
J1640+2224	0.003163	175.461	0.000797	0.25	0.000096
J1708−3506	0.004505	149.133	0.000244	0.16	0.000230
J1643−1224	0.004622	147.017	0.000505	0.12	0.000296
J2302+4442	0.005192	125.935	0.000503	0.29	0.000266
J1529−3828	0.008486	119.675	0.000168	0.16	0.000484
B1953+29	0.006133	117.349	0.000330	0.18	0.000432
J1853+1303	0.004092	115.654	0.000023	0.24	0.000191
J1751−2857	0.003915	110.746	0.000128	0.19	0.000212
J2229+2643	0.002978	93.016	0.000255	0.12	0.000067
J1935+1726	0.004200	90.764	0.000175	0.22	–
J1850+0124	0.003560	84.950	0.000069	0.25	0.000199
J1737−0811	0.004175	79.517	0.000053	0.07	0.000184
J2019+2425	0.003935	76.512	0.000111	0.31	0.000168
J1125−5825	0.003102	76.403	0.000257	0.26	0.000440
J1455−3330	0.007987	76.175	0.000170	0.25	0.000446
J1713+0747	0.004570	67.825	0.000074	0.28	0.000230
J1910+1256	0.004984	58.467	0.000230	0.19	0.000222
J2033+1734	0.005949	56.308	0.000128	0.19	0.000260
J0614−3329	0.003149	53.585	0.000180	0.28	0.000238
J1825−0319	0.004554	52.630	0.000193	0.18	0.000178
J1844+0115	0.004186	50.646	0.000257	0.14	0.000214

Table 5. Parameters of the glitches of PSRs J0611+1436 and J1907+0631[a]

	PSR J0611+1436	PSR J1907+0631
R.A. (J2000)	06:11:18.649(13)	19:07:03.82(2)
Decl. (J2000)	+14:36:52(4)	+6:31:18.9(6)
Pulsar rotation frequency (s^{-1})	3.6991898114(6)	3.0897763136(2)
Pulsar frequency first derivative (s^{-2})	$-51.37(1) \times 10^{-15}$	$-4316.60(1) \times 10^{-15}$
Epoch of pulsar frequency (MJD)	55818	56378.03
Glitch epoch (MJD)	55817.8	56985
Glitch frequency increment (s^{-1})	$2.0624(2) \times 10^{-5}$	$6.495(2) \times 10^{-6}$
Glitch frequency first derivative increment (s^{-2})	$-0.03(2) \times 10^{-15}$	$-20.9(3) \times 10^{-15}$
Spin-down age (kyr)	1070	11.3
Spin-down energy (erg/s/10^{32})	80	5300
Inferred Magnetic Field (G/10^{12})	1.05	12.2

[a]Figures in parentheses are uncertainties in the last digit quoted.